Excited-state dynamics of $[Mn(im)(CO)_3(phen)]^+$: PhotoCORM, catalyst, luminescent probe?

Maria Fumanal, Chantal Daniel, Etienne Gindensperger*

Laboratoire de Chimie Quantique, Institut de Chimie Strasbourg, UMR-7177 CNRS/Université de Strasbourg, 1 Rue Blaise Pascal BP 296/R8, F-67008 Strasbourg, France.

ABSTRACT

Mn(I) α-diimine carbonyl complexes have shown promise in the development of luminescent CO release materials (photoCORM) for diagnostic and medical applications due to their ability to balance the energy of the low-lying metal-to-ligand charge transfer (MLCT) and metal-centered (MC) states. In this work, the excited state dynamics of $[Mn(im)(CO)_3(phen)]^+$ (im = imidazole; phen = 1,10-phenanthroline) is investigated by means of wavepacket propagation on the potential energy surfaces associated to the eleven low-lying S_n singlet excited states within a vibronic coupling model in a (quasi) diabatic representation including sixteen nuclear degrees of freedom. The results show that the early time photophysics (< 400 fs) is controlled by the interaction between two MC dissociative states, namely S_5 and S_{11}, with the lowest S_1-S_3 MLCT bound states. In particular, the presence of S_1/S_5 and S_2/S_{11} crossings within the diabatic picture along the $Mn\text{-}CO_{axial}$ dissociative coordinate ($q_{Mn\text{-}COaxial}$) favours a two-stepwise population of the dissociative states, at about 60-70 fs (S_{11}) and 160-180 fs (S_5), that reaches about 10% within 200 fs. The one-dimensional reduced densities associated to the dissociative states along $q_{Mn\text{-}COaxial}$ as function of time clearly point to concurrent primary processes, namely CO release vs. entrapping into the S_1 and S_2 potential wells of the lowest luminescent MLCT states within 400 fs, characteristics of luminescent photoCORM.

* Author to whom correspondence should be addressed: egindensperger@unistra.fr

I. INTRODUCTION

The discovery of photoactive 1st row transition metal complexes under visible light with both fluorescence and photo-induced release carbonyl material (photoCORM) behaviours is crucial for the development of theranostic agents for cancer therapy and near-IR imaging.[1-3] Whereas suitable luminescent activity is stimulated by visible light in rhenium (I) α-diimine carbonyl complexes for efficient probing in various environments, carbonyl release needs UV irradiation in these 3rd row complexes because of the destabilization of the metal-centred (MC) excited states.[4-6] In contrast 1st row analogous, hardly activated by visible light, may easily loss a carbonyl ligand via ultrafast processes (< 100 fs) quenching the luminescent process. Recent experimental research interest in this field leads to the synthesis of novel compounds, functionalized from early Re(I) and Mn(I) α-diimine complexes, suitable for bio-medical applications.[7-10] Within the context of CO_2 reduction catalysis, ultrafast spectroscopy of $[MnBr(CO)_3(R\text{-bpy})]$ (R-bpy = 4,4'-disubstituted 2,2'-bipyridyl; R= ^{t}Bu, H, CF_3, NO_2) has been investigated in acetonitrile. This recent study points to a time constant for CO release of 460-680 fs, sensitive to the R substituent, subsequent solvent coordination occurring within 18 to 39 ps time scale.[11]

In our quest for a deep understanding of the early-time excited-state dynamics in $[M(L)(CO)_3(N,N)^n$ (M = Mn, Re; L= halide, imidazole; N,N = phenanthroline, bipyridine), we have investigated a number of molecules in solution by means of electronic structure theory[12-15] and non-adiabatic quantum dynamics.[16-21] In particular we have studied the role of the surrounding ligands L and of the metal centre on the excited state dynamics. We have shown that ultrafast decay, within the first picosecond (ps), is driven by a spin-vibronic mechanism[22] where spin-orbit coupling (SOC) and vibronic effects play a central role but not always as expected from the classical "cascade" concept of intersystem crossing (ISC) and internal conversion (IC). Comparing the photophysics of $[Re(im)(CO)_3(phen)]^+$ and $[Mn(im)(CO)_3(phen)]^+$ it has been shown[21] that the early time photophysics (< 200 fs) of the rhenium complex, namely an ultrafast decay from the S_2 MLCT (metal-to-ligand-charge-transfer) absorbing state to T_3 an intermediate IL_{phen} (intra ligand) state, is mainly driven by SOC. Vibronic effects activated by CO and phen motions are involved in the subsequent transfer of population from T_3 to the long-lived T_1 ^{3}MLCT excited state.[19] In contrast the high density of excited state and the presence of low-lying MC states in the manganese analogous modifies drastically the dynamics with an ultrafast S_2 to S_1 internal conversion and a minor population of the low-lying triplet states in the first ps.[21] The investigation of the adiabatic PES

associated to S_2 and S_1 of $[Mn(im)(CO)_3(phen)]^+$ point to a potentially fluorescent state calculated at 570 nm and highly competitive deactivation channels, namely the CO loss and the imidazole dissociation.[15]

Whereas previously reported non-adiabatic quantum dynamics simulations have been successful in deciphering ultrafast photophysical processes in 1st-row transition metal complexes[23-27,21] their use to follow competitive photo induced processes is still challenging. Recent simulations are mostly devoted to isomerization, fragmentation or charge transfer in organic chromophores.[28-30] Simulations of quantum dynamics including dissociative coordinates[31] are still scarce and only one example has been reported for a 1st-row transition metal complex, namely the ultrafast photolysis of the heme-CO complex.[32]

The present study is devoted to quantum dynamics simulations capable to follow the competition between fluorescence and carbonyl loss in $[Mn(im)(CO)_3(phen)]^+$, in particular the axial carbonyl, see Scheme 1. The next Section describes the vibronic model constructed to study this molecule as well as the methodology used. The results obtained are then discussed and put in perspective with experimental findings on related Mn(I) complexes.

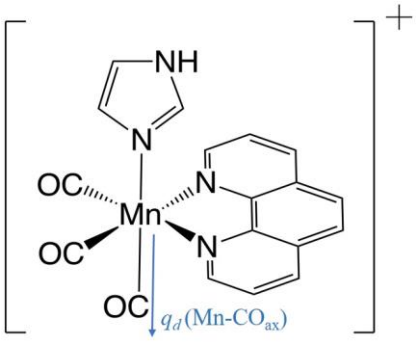

Scheme 1. Structure of $[Mn(im)(CO)_3(phen)]^+$ together with the axial CO release mode, q_d (Mn-CO$_{ax}$).

II. METHOD AND MODEL

In order to study the excited-state quantum dynamics of $[Mn(im)(CO)_3(phen)]^+$ we construct a vibronic coupling Hamiltonian in a (quasi) diabatic representation,[33-35] and use similar mathematical functions for the potential energy surfaces as in Ref [32]. Our approach is based on mass- and frequency-weighted (dimensionless) normal modes q_i as coordinate system, in addition to the Mn-CO$_{ax}$ distance q_d (with unit length.)

The Hamiltonian reads:

$$\boldsymbol{H}(\boldsymbol{q}) = T(\boldsymbol{q})\mathbf{1} + \boldsymbol{W}(\boldsymbol{q}) \quad (1)$$

where bold symbols represent matrices. $T(\boldsymbol{q})$ is the kinetic energy and $\boldsymbol{W}(\boldsymbol{q})$ the diabatic potential energy matrix including the non-adiabatic coupling. **1** is the unit matrix. The elements $W^{(nm)}(\boldsymbol{q})$ of $\boldsymbol{W}(\boldsymbol{q})$ are:

$$W^{(nm)}(\boldsymbol{q}) = \sum_i W_i^{(nm)}(q_i) + W_d^{(nm)}(q_d) + \delta_{nm}E_n \quad (2)$$

with E_n the vertical transition energy for the state n and $W_i^{(nm)}(q_i)$ consisting of the linear vibronic coupling terms:[33]

$$W_i^{(nm)}(q_i) = \delta_{nm}\frac{\omega_i}{2}{q_i}^2 + \kappa_i^{(nm)}q_i \quad (3)$$

where ω_i is the ground-state vibrational frequency of mode i and $\kappa_i^{(nm)}$ is the intrastate (for n=m) or interstate (for n≠m) coupling constant. In addition,

$$W_d^{(nm)}(q_d) = \kappa_d^{(nm)}(q_d) + \delta_{nm}f_n(q_d) \quad (4)$$

with

$$f_n(q_d) = \alpha_n e^{\beta_n(q_d - q_{d_n})} \quad \text{(dissociative), or} \quad (5)$$

$$f_n(q_d) = D_n(1 - e^{\gamma_n(q_d - q_{d_n})})^2 \quad \text{(Morse)} \quad (6)$$

i.e. along q_d the potential energy is given either by an exponential function to describe dissociative states, or a Morse potential for bound states. The coupling $\kappa_d^{(nm)}(q_d)$ contains a function which switches off the interstate coupling as q_d increases to avoid unphysical coupling at large q_d.

The parameters entering the Hamiltonian for the excited-state dynamics of $[Mn(im)(CO)_3(phen)]^+$ are obtained from quantum chemistry. Electronic structure calculations were performed under Cs symmetry by means of Density Functional Theory (DFT) including water solvent corrections based on a conductor-like screening model (COSMO).[36-38] The

calculations were performed using the B3LYP functional[39] and all electron triple-ζ basis set.[40] The scalar relativistic effects were taken into account within the zeroth-order regular approximation (ZORA).[41]

The reference Frank-Condon geometry of $[Mn(im)(CO)_3(phen)]^+$ was obtained at the DFT level stated above by first optimizing the pentacoordinate $[Mn(im)(CO)_2(phen)]^+$ system without the axial CO under Cs symmetry. The normal modes of this structure were used as the basis for the linear vibronic coupling model part of the model along the q_i. In a second step, the position of the axial CO was optimized in the $[Mn(im)(CO)_3(phen)]^+$ complex by keeping all other degrees of freedom fixed. In this way, we decoupled all internal degrees of freedom of $[Mn(im)(CO)_3(phen)]^+$ from the axial CO dissociation coordinate. This approximation was possible because the optimized geometry of $[Mn(im)(CO)_2(phen)]^+$ remains mostly unperturbed from the fully coordinated $[Mn(im)(CO)_3(phen)]^+$. But, of course, anharmonic coupling between modes and between q_i and q_d, nor Dushinsky rotation, are in turn not included in our model so far.

The vertical transition energies E_n of the 11 lowest singlet excited states (5 A' and 6 A") were computed within TD-DFT[42-43] at the same level described above under the Tamm-Dancoff approximation (TDA).[44] The nonequilibrium solvation within the linear-response TD-DFT with a high-frequency dielectric constant of 1.77 for water is used. The SOC effects were introduced according to a simplified relativistic perturbative TD-DFT formalism.[45-46] However, the SOC effect is minor in this Mn complex and triplet states play a minor role on the early time dynamics[21] and are thus excluded in the present study. The vertical excited state manifold of the reference geometry of $[Mn(im)(CO)_3(phen)]^+$ and that of the fully optimized complex as reported in Ref. [21] are very similar, see Supplementary material, Table S1. The vertical transition energies used here are reported in Table 1 for the 5 A' and 6 A'' states.

State	E_{vert}	E_{min}[(a)]	E_{reorg}[(a)]
S1(A")	3.10	2.75	0.35
S2(A')	3.39	3.20	0.19
S3(A')	3.49	3.31	0.18
S4(A')	3.57	3.29	0.28
S5(A")	3.64	3.27	0.37
S6(A')	3.65	3.32	0.33
S7(A")	3.73	3.51	0.22

S8(A")	3.79	3.29	0.50
S9(A")	3.91	3.66	0.25
S10(A")	3.93	3.68	0.25
S11(A')	4.01	3.64	0.37

Table 1. Excited-state energies in eV and symmetry of the 11 electronic states (5 A' and 6 A'') included in the model Hamiltonian for $[Mn(im)(CO)_3(phen)]^+$. E_{vert} is the vertical transition energy. E_{reorg} is the reorganisation energy and $E_{min} = E_{vert} - E_{reorg}$. (a) Notice that only the intrastate contribution is included, see text for details.

Intrastate vibronic coupling values $\kappa_i^{(nn)}$ were obtained by calculating the analytical gradients of the excited states of the reference $[Mn(im)(CO)_3(phen)]^+$ geometry excluding the contributions of the axial CO group. Interstate coupling values $\kappa_i^{(n\neq m)}$ were obtained using the overlap approach in which the vibronic coupling values are extracted from the overlap of the excited state wave-functions at displaced geometries at q_i=0.1 along the selected normal modes.[47] Based on an analysis of the strength of the coupling, we have selected 12 totally symmetric modes (a') and 3 non-totally symmetric modes (a'') to enter the dynamics. The coupling constants of these modes are not fitted, but rather extracted directly from the electronic structure data. Along with the dissociative (a') coordinate along the Mn-CO_{axial} bond, the dynamics include a total of 16 degrees of freedom and 11 states. Note that the excited state dynamics of $[Mn(im)(CO)_3(phen)]^+$ computed from the fully optimized bounded model as reported in Ref. [21] and that computed for the reference complex studied here (assuming a bounded harmonic potential along q_d for comparison) agree very well in showing ultrafast internal conversion from S_2 to S_1 at early timescales (see Supplementary material, Fig. S2), suggesting that our strategy to extract the parameters is valid.

To represent the dissociative channel, TD-DFT/TDA calculations were performed along the axial CO coordinate by elongating the Mn-CO distance q_d. Among the 11 electronic states included here, two of them are dissociative upon Mn-CO elongation, namely S_5(A'') and S_{11}(A'), both of MC character. All other states are bound and of MLCT character mainly. See Supplementary material Fig. S1 for electron density differences at FC and CO_{ax} dissociation for selected states. The absorbing state is S_2(A'). The obtained excited state potentials were then diabatized by *ansatz* and the corresponding parameters fitted to the dissociative and Morse functions as in Eqs. (4-6) above. The shape of the potential energy curve and states associated with them are discussed in more details in the next section.

All electronic structure calculations were done with ADF2013 code.[48] The quantum dynamics calculations were performed with the Multiconfiguration Time-Dependent Hartree method[49-51] (MCTDH, Heidelberg Package version 8.4.13.)[52]

III. RESULTS AND DISCUSSION

The optical absorption properties of $[Mn(im)(CO)_3(phen)]^+$ have been discussed in detail in Ref. [15] and are only summarized here for latter reference. The experimental absorption spectrum of $[Mn(im)(CO)_3(phen)]^+$ in CH_2Cl_2 shows a broad peak at 380 nm which is ascribed to low-lying MLCT transitions.[53] The calculated spectra for the Cs conformer displays three low-lying peaks at 329, 349 and 365 nm, the latter corresponding to the lowest absorbing S_2 state mainly characterized as a $MLCT_{phen}$ transition.

In order to assess the possibility of fluorescence in this complex, the minima of excited states have been calculated. TD-DFT/TDA geometry optimizations of the lowest lying S_1 and S_2 states of $[Mn(im)(CO)_3(phen)]^+$ in water lead both to bounded minima at 2.43 eV and 2.98 eV with respect to the ground state minimum, respectively, as reported in Ref [15] indicating that these MLCT states will be emissive upon excitation. However, previous state correlation diagrams, and a throughout exploration of the minimum energy conical intersections (MECI), showed low-lying crossing points between S_1 and S_2 and two upper states (S_5 and S_{11}) of MC character along the axial CO dissociation coordinate, the most favourable dissociative pathway on energetic basis. This suggests that competitive CO release is promoted at the crossing points upon excitation, in agreement with the experimental literature. To address this question, excited state dynamics simulations are performed incorporating the axial CO dissociation channel, going beyond the bounded model previously reported.[21]

The quantum dynamics is performed in the diabatic representation. The associated potential energy curves along q_d, the Mn-CO_{axial} distance, are represented in Fig. 1. All other modes are kept to their ground state equilibrium value ($q_i = 0$). The top panel shows the diabatic curves, while the bottom panel shows the corresponding adiabatic curves as obtained by the diagonalization of the coupling matrix $\boldsymbol{W}(\boldsymbol{q})$, see Eq. (2). It can be seen that the dissociative curves S_5 and S_{11} cross the bound states in the diabatic picture. The strong interaction between S_1(A'') and S_5(A'') along q_d creates a barrier in the lowest lying adiabatic state at about 2.2 Å, where the MC character leading to dissociation then dominates. Similar mixing, *albeit* not that strong, occurs between S_2(A') and S_{11}(A'). S_1(A'') is significantly coupled to S_2(A') and S_3(A') along non-totally symmetric a'' modes. However the coupling

between S_2(A') and S_3(A') with S_5(A'') along a'' modes is weak. This will have consequences on the dissociation dynamics as we shall discuss further below. We have also evaluated the reorganization energy due to the intrastate contributions of all totally symmetric modes (see Table 1). The value for S_1, S_5 and S_{11} is very similar at about 0.35 eV, while that of S_2 is smaller at only 0.2 eV. The smaller stabilization of S_2 will impact the dynamics as well. A comparison between the TD-DFT calculated adiabatic potentials and the adiabatic curves extracted from our model shows a good agreement in the energy domain considered here (below 3.6 eV, see Supplementary material Fig. S3.)

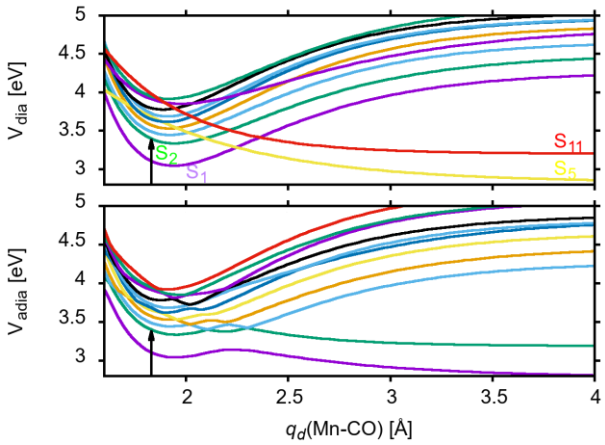

Figure 1. Diabatic (top) and adiabatic (bottom) potential energy curves along the Mn-CO distance. The arrow indicates the vertical transition to S_2. The adiabatic curves are obtained by diagonalization of the diabatic matrix $\boldsymbol{W}(\boldsymbol{q})$.

In order to evaluate the dissociation rate of the axial CO, we computed the diabatic population of the electronic states as a function of time. The results obtained from the 16-modes 11-states MCTDH calculation are shown in Fig. 2.

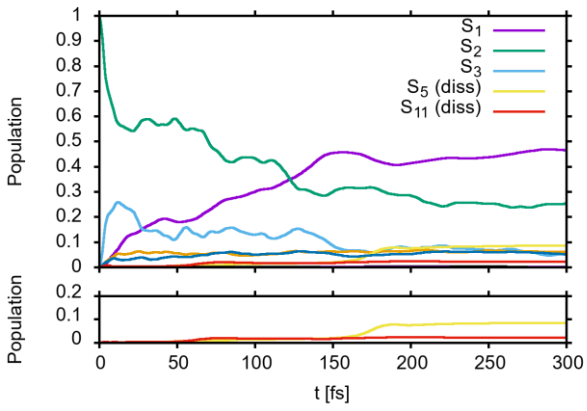

Figure 2. Diabatic electronic populations as a function of time after initial population of S_2. The population of S_5 and S_{11} is an estimate of the dissociation probability, which is about 10%. S_2 and S_3 exchange population during their decay to S_1. The tail shows only the population of S_5 and S_{11}.

The initial population of S_2 quickly drops in about 10 fs to transiently populate S_3, which lies only 0.1 eV above S_2 at the Franck-Condon geometry (see Table 1.) Then population exchange between these states occurs, as manifested by the oscillations in the populations. Altogether, the population of S_2 and S_3 decay mainly to S_1, which is significantly populated after 150 fs.

The two dissociative states S_5 and S_{11} are only marginally populated. A small amount of population in both S_5 and S_{11} occurs at about 60-70 fs. Then, the population of S_5 increases stepwise at about 160-180 fs. The population of these two states then remain constant at least until 500 fs, our calculation time (only the first 300 fs are shown in Fig. 2.) The cumulative population of S_5 and S_{11} provides an estimate of the dissociation probability, which is about 10% within 200 fs. Some other states are slightly populated during the dynamics but do play a role in the relaxation process.[21]

The low dissociation probability can be explained by the weak S_2/S_5 coupling along a'' modes. Whereas S_2 is significantly coupled to S_{11} along the a' dissociative coordinate q_d, its crossing with S_{11} is high in energy, and consequently not strongly active (Fig. 1, top.) The energy of the S_2/S_{11} crossing is at 3.51 eV (or at 3.34 eV considering the reorganization energy, *i.e.* 0.14 eV above S2 minimum, see Table 1.) In addition, the strong coupling between S_1 and S_5 can be efficient only once S_1 is significantly populated (~150 fs) (Fig. 2), but within this time scale the molecular complex may relax to the S_1 minimum, where the coupling is weaker. The coupling is maximum at the intersection between S_1 and S_5 diabatic potentials (or the barrier in the adiabatic representation), which is at about 2.2 Å along q_d, roughly 0.3 Å away from the S_1 minimum and where the S_1/S_5 population transfer occurs. The energy of this S_1/S_5 crossing is evaluated at 3.28 eV, *i.e.* more than 0.2 eV from the S1 minimum. The analysis of the 1D-reduced density along q_d as a function of time as shown in Fig. 3 is in favor of this explanation, as developed below.

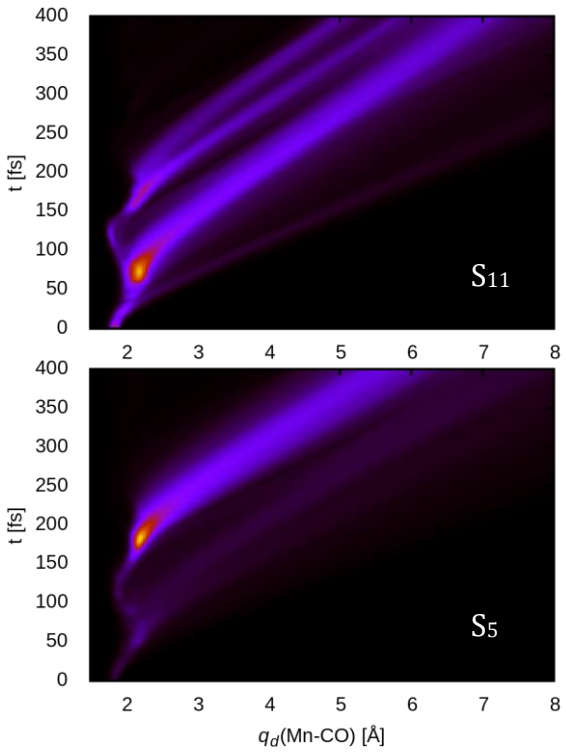

Figure 3. 1D reduced density along q_d as a function of time for the two dissociative states. Upper panel: on the S_{11} state; Lower panel: on the S_5 state. The color coding indicates the value of the density, from zero (black) to low (purple-blue) to more important (red then yellow) values. Note that the scale of the color coding is not the same in the two panels. The density for q_d > 2.2 Angström represents the CO dissociation.

To analyse this figure, let us first divide each panel into two parts, one for q_d < 2.2 Å, *i.e.* before the crossings of S_1/S_5 and S_2/S_{11} (or the adiabatic barriers) and one for q_d > 2.2 Å which represents the part of the wavepacket corresponding to the axial CO dissociation. In the "bounded" part, we can identify oscillations of a period of about 120 fs, which corresponds to the motion of the wavepacket in S_1, S_2 and S_3 –which appears to be evolving rather like a classical coherent state. Notice that the initial wavepacket is located at the inner turning point of S_2 (see the arrow in Fig. 1.) After half a period, *i.e.* about 60 fs, the wavepacket reaches its outer turning point, where the coupling is maximal, and where the population transfer to the dissociative states occurs. For S_{11} (Fig. 3, top), which is mainly coupled to S_2 and S_3, this happens at 60 fs with a strong intensity and at 180 fs to a lower extend. After that time, the S_2 (and S_3) population has dropped and relaxed; see Fig. 2, cancelling any further population transfer to S_{11}. For S_5 (Fig. 3, bottom), we do see a small part of the wavepacket starting to

dissociate after 60 fs, but the most intense population transfer occurs once S_1 is significantly populated and the wavepacket in S_1 reaches its outer turning point, *i.e.* at 180 fs. Then, S_1 relaxes to its minimum, leaving the crossing to S_5 inefficient and the dissociation process stops. The population remaining in S_1 will allow for fluorescence and/or possibly further dissociation of the two remaining equatorial carbonyls. The scenario depicted above is controlled by the position of the critical points (energy minima and crossings) on the potential energy surfaces. In the present case two channels are clearly open after irradiation at ~ 400 nm as observed experimentally for the luminescent Mn photoCORM $[Mn(imdansyl)(CO)_3(phen)]^+$ (imdansyl = dansylimidazole) proposed by Jimenez *et al.*,[2] namely CO release and fluorescence. Modifying the α-diimine ligand or varying phenanthroline substituents may quench one or the other channels tailoring either pure stable catalysts or efficient luminescent probes.

As far as the dissociation of remaining carbonyls is concerned it has been shown experimentally on related Mn-tricarbonyl complexes,[11] and theoretically from our static exploration[15] of the dissociative channels of $[Mn(im)(CO)_3(phen)]^+$ that not only the axial CO can dissociate, but also the equatorial carbonyls. Of course, including the dissociation of the equatorial carbonyls in the quantum dynamics would be of prime interest. Unfortunately, the construction of a meaningful model is extremely complicated, including multiple dissociation channels and considering the lack of symmetry and large amount of electronic states involved.

IV. CONCLUSIONS AND OUTLOOK

Simulation of excited state quantum dynamics of $[Mn(im)(CO)_3(phen)]^+$ based on vibronic coupling model including eleven singlet electronic states and fifteen normal modes, in addition to the axial carbonyl dissociative one, has enabled to propose a semi-quantitative mechanism for the competitive process that characterizes photoCORM based on manganese complexes. After irradiation at about 400 nm the initially populated MLCT state (S_2) efficient population transfer to S_3, in less than 20 fs, is observed, whereas the lowest MLCT state (S_1) is efficiently populated to reach 45% within 150 fs. A two stepwise process populates upper MC states, at 60-70 fs and 160-180 fs leading to an overall dissociation probability of 10% within 200 fs. Then the system may either be trapped into the S_1 potential well for further luminescent process, or decay along other dissociative channels involving equatorial CO or imidazole. Moreover, at longer time scales the role of the triplet states, as well as solvent molecules cannot be excluded. By modifying the imidazole and phenanthroline ligands, not only the relative position of the MLCT and MC states will be affected, but also the barrier energy highs (position

of the minimum energy crossings) and the vibronic effects via the active normal modes. The vibronic model Hamiltonian presented here for ultrafast excited state dynamics (< 400 fs) in a first-row transition metal complex can be adapted to different chemical situations, in term of MC/MLCT relative stability and interaction, as long as reliable electronic structure data are available. Investigation of longer time scales should include not only spin-orbit coupling, but also additional coordinates (equatorial carbonyls, solvent).

SUPPLEMENTARY MATERIAL

See the supplementary material for the optimized structures and vertical transition energies used in this and our previous work. Comparison of the dynamics of the two models (bounded versions.) Comparison of the model and calculated (TD-DFT) adiabatic potential energy curves. Electron density differences at FC and CO_{ax} dissociation.

ACKNOWLEGMENT

This work has been supported by Labex CSC (ANR-10-LABX-0026_CSC). We thank G. Worth, C. Micicoi and E. Louis for fruitful discussions. The calculations have been performed at the High Performance Computer Centre (HPC), University of Strasbourg and on the nodes cluster of the Laboratoire de Chimie Quantique.

DATA AVAILABILITY

The data that support the findings of this study are available from the corresponding author upon reasonable request.

REFERENCES

[1]J. Jimenez, I. Chakraborty, S. J. Carrington, P. K. Mascharak, Dalton Trans. **45**, 13204 (2016).

[2]J. Jiminez, I. Chakraborty, A. Dominguez, J. Martinez-Gonzalez, W. M. C. Sameera, P. K. Mascharak, Inorg. Chem. **57**, 1766 (2018).

[3]J. Jimenez, M. N. Pinto, J. Martinez-Gonzalez, P. K. Mascharak, Inorganica Chimica Acta **485**, 122 (2019).

[4]S. J. Carrington, I. Chakraborty, J. M. C. Bernard, P. K. Mascharak, Inorg. Chem. **55**, 7852 (2016).

[5]I. Chakraborty, S. J. Carrington, G. Roseman, P. K. Mascharak, Inorg. Chem. **56**, 1534 (2017).

[6]I. Chakraborty, J. Jimenez, W. M. C. Sameera, M. Kato, P. K. Mascharak, Inorg. Chem. **56**, 2863 (2017).

[7]M. N. Pinto, I. Chkraborty, J. Jimenez, K. Murphy, J. Wenger, P. K. Mascharak, Inorg. Chem. **58**, 14522 (2019).

[8]Q. Jiang, Y. Xia, J. Barrett, A. Mikhailovsky, G. Wu, D. Wang, P. Shi, P. C. Ford, Inorg. Chem. **58**, 11066 (2019).

[9]M. N. Pinto, P. K. Mascharak, J. Photochem. Photobio. C: Photochemistry Review **42**, 100431 (2020).

[10]B. Kawahara, L. Gao, C. Janzen, P. K. Mascharak, Chem. Sci. **1**, 467 (2020).

[11] W. C. Henke, C. J. Otolski, W. N. G. Moore, C. G. Elles, J. D. Blakemore, Inorg. Chem. **59**, 2178 (2020).

[12]M. Fumanal, C. Daniel, J. Comp. Chem. **37**, 2454 (2016**).**

[13]M. Fumanal, C. Daniel, J. Phys. Chem. A **120**, 6934 (2016)**.**

[14]S. Mai, H. Gattuso, M. Fumanal, A. Muñoz-Losa, A. Monari, C. Daniel, L. Gonzalez, Phys. Chem. Chem. Phys. **19**, 27240 (2017).

[15]M. Fumanal, Y. Harabuchi, E. Gindensperger, S. Maeda, C. Daniel, J. Comput. Chem. **40**, 72 (2019).

[16]J. Eng, C. Gourlaouen, E. Gindensperger, C. Daniel, Acc. Chem. Res. **48**, 809 (2015).

[17]C. Gourlaouen, J. Eng, M. Otsuka, E. Gindensperger, C. Daniel, J. Chem. Theor. Comp. **11**, 99 (2015).

[18]Y. Harabuchi, J. Eng, E. Gindensperger, T. Taketsugu, S. Maeda, C. Daniel, J. Chem. Theory Comput. **12**, 2335 (2016).

[19]M. Fumanal, E. Gindensperger, C. Daniel, J. Chem. Theory Comput. **13**, 1293, (2017).

[20]M. Fumanal, E. Gindensperger, C. Daniel, Phys. Chem. Chem. Phys. **20**, 1134 (2018).

[21]M. Fumanal, E. Gindensperger, C. Daniel, J. Phys. Chem. Lett. **9**, 5189 (2018).

[22]T. J. Penfold, E. Gindensperger, C. Daniel, C. M. Marian, Chem. Rev. **118**, 6975 (2018).

[23]M. Pápai, G. Vankó, T. Rozgonyi, T. J. Penfold, J. Phys. Chem. Lett. **7**, 2009 (2016).

[24]M. Pápai, T. Rozgonyi, T. J. Penfold, M. N. Nielsen, K. B. Møller, J. Chem. Phys. **151**, 104307 (2019).

[25]M. Pápai, M. Simmermacher, T. J. Penfold, K. B. Møller, J. Chem. Theory Comput. **14**, 3967 (2018).

[26]M. Pápai, M. Abedi, G. Levi, E. Biasin, M. M.Nielsen, K. B. Moller, J. Phys. Chem. C **123**, 2056 (2019).

[27]G. Capano, M.Chergui, U. Rothlisberger, I. Tavernelli, T. J. Penfold, J. Phys. Chem. A **118**, 9861 (2014).

[28]J. L. Woodhouse, M. Assmann, M. A. Parkes, H. Grounds, S. J. Pacman, J. C. Anderson, G. A. Worth, H. H. Fielding, Phys. Chem. Chem. Phys. **19**, 22711 (2017).

[29]K. E. Spinlove, M. Vacher, M. Bearpark, M. A. Robb, G. A. Worth, Chem. Phys. **482**, 52 (2017).

[30]C. Robertson, G. A. Worth, Chem. Phys. **510**, 17 (2018).

[31]C. Robertson, G. A. Worth, Phys. Chem. Chem. Phys. **19**, 29483 (2017).

[32]K. Falahati, H. Tamura, I. Burghardt, M. Huix-Rotlant, Nature Commun. **9**, 4502 (2018).

[33]H. Köppel, W. Domcke, L. S. Cederbaum, Adv. Chem. Phys. **57**, 59 (1984).

[34]G. Worth, L. S. Cederbaum, Ann. Rev. Phys. Chem. **55**, 127 (2004).

[35]G. Worth, H. Köppel, E. Gindensperger, L. S. Cederbaum, in Multidimensional Quantum Dynamics, H.-D. Meyer, F. Gatti and G. Worth, Eds. (Wiley-VCH, Weinheim, 2009)

[36]A. Klamt, A., G. J. Schüürmann, Chem. Soc., Perkin Trans. 2, **2**, 799 (1993).

[37]A. Klamt, J. Phys. Chem. **99**, 2224 (1995).

[38]A. Klamt, A., V. Jonas, J. Chem. Phys. **105**, 9972 (1996).

[39]P. J. Stephens, F. J. Devlin, C. F. Chabalowski, M. J. Frisch, J. Phys. Chem. **98**, 11623 (1994).

[40]E. Van Lenthe, E. J. Baerends, J. Comput. Chem. **24**, 1142 (2003).

[41]E. Van Lenthe, R. Van Leeuwen, E. J. Baerends, J. G. Snijders, Int. J. Quantum Chem. **57**, 281 (1996).

[42]E. Runge, E. K. U. Gross, Phys. Rev. Lett. **52**, 997 (1984).

[43]M. Petersilka, U. J. Gossmann, E. K. U. Gross, Phys. Rev. Lett. **76**, 1212 (1996).

[44]M. J. Peach, D. J. Tozer, J. Phys. Chem. A **116**, 9783 (2012).

[45]F. Wang, T. Ziegler, E. van Lenthe, S. J. A. van Gisbergen, E. J. Baerends, J. Chem. Phys. **112**, 204103 (2005).

[46]F. Wang, T. Ziegler, J. Chem. Phys. **113**, 154102 (2005).

[47]M. Fumanal, F. Plasser, S. Mai, C. Daniel, E. Gindensperger, J. Chem. Phys. **148**, 124119 (2018).

[48]ADF, SCM, Theoretical Chemistry, Vrije Universiteit, Amsterdam, The Netherlands (2013). Online at https://www.scm.com/Downloads/.

[49]H.-D. Meyer, U. Manthe, L. S. Cederbaum, Chem. Phys. Lett. **165**, 73 (1990).

[50]M. H. Beck, A. Jaĉkle, G. A. Worth, H.-D. Meyer, H. −D. Phys. Rep. **324**, 1 (2000).

[51]H.-D. Meyer, F. Gatti, G. A.Worth, Eds., Multidimensional Quantum Dynamics: MCTDH Theory and Applications; Wiley-VCH: Weinheim, Germany (2009).

[52]G. A. Worth, M. H. Beck, A. Jäckle, H.-D. Meyer. The MCTDH Package, Version 8.2 (2000), University of Heidelberg, Heidelberg, Germany. H.-D. Meyer, Version 8.3 (2002), Version 8.4 (2007). O. Vendrell, H.-D. Meyer, Version 8.5 (2011). See http://mctdh.uni-hd.de.

[53]I. de Aguiar, F. C.A. Lima, J. Ellena,V. R.S. Malta, R. M. Carlos, Comp. Theor. Chem. **965**, 7 (2011).